TISSUE ENGINEERING: Part A
Volume 15, Number 8, 2009

DOI: 10.1089/ten.tea.2008.0430

Original Article

Increased Myocyte Content and Mechanical Function Within a Tissue-Engineered Myocardial Patch Following Implantation

Damon J. Kelly, Ph.D.,[1,2] Amy B. Rosen, Ph.D.,[3] Adam J.T. Schuldt, Ph.D.,[3]
Paul V. Kochupura, M.D.,[4] Sergey V. Doronin, Ph.D.,[1,5] Irina A. Potapova, Ph.D.,[1,5]
Evren U. Azeloglu, Ph.D.,[6] Stephen F. Badylak, M.D., Ph.D., D.V.M.,[7] Peter R. Brink, Ph.D.,[1,5]
Ira S. Cohen, M.D., Ph.D.,[1,5] and Glenn R. Gaudette, Ph.D.[8]

During the past few years, studies involving the implantation of stem cells, chemical factors, and scaffolds have demonstrated the ability to augment the mammalian heart's native regenerative capacity. Scaffolds comprised of extracellular matrix (ECM) have been used to repair myocardial defects. These scaffolds become populated with myocytes and provide regional contractile function, but quantification of the myocyte population has not yet been conducted. The purpose of this study was to quantitate the myocyte content within the ECM bioscaffold and to correlate this cell population with the regional mechanical function over time. Xenogenic ECM scaffolds derived from porcine urinary bladder were implanted into a full-thickness, surgically induced, right ventricular-free wall defect in a dog model. Zero, 2, and 8 weeks following implantation, regional function and myocyte content were determined in each patch region. Regional function did not significantly increase from 0 to 2 weeks. At 8 weeks, however, regional stroke work increased to $3.7 \pm 0.7\%$ and systolic contraction increased to $4.4 \pm 1.2\%$. The myocyte content also significantly increased during that period generating a linear relationship between regional function and myocyte content. In conclusion, ECM used as a myocardial patch increases both the regional function and the myocyte content over time. The mechanical function generated in the patch region is correlated with the quantity of local tissue myocytes.

Introduction

Dacron (polyethylene terephthalate), Gore-Tex (polytetrafluoroethylene), and glutaraldehyde-treated bovine or human pericardium are currently used for repair of congenital or acquired myocardial defects and replacement of postinfarct akinetic or dyskinetic myocardium.[1–3] While these materials effectively provide mechanical stability in place of compromised myocardium, they induce a fibrotic host tissue response, do not resorb over time, and do not contribute contractile function.[4,5] A material that could support regeneration of functional myocardium would improve cardiac function over the currently used materials.

Acellular extracellular matrix (ECM) derived from porcine urinary bladder has been used successfully to repair defects in canine and porcine right ventricles[4,6] and in porcine left ventricles.[7] These studies demonstrate that when used as a myocardial patch, ECM scaffolds that are not chemically crosslinked provide regional contractile function and become populated with islands of myocytes 8 weeks postimplantation, while Dacron does neither. Immediately following implantation, ECM demonstrates no regional stroke work (RSW) and negative systolic contraction (SC), due to its greater compliance than neighboring myocardium, but proceeds to generate positive RSW and SC 8 weeks postimplantation. This is associated with cellularization and population by islands of myocytes.[8]

This study addresses the question of whether the increase in contractile function generated by the ECM region over 8 weeks correlates with an increase in myocyte quantity over the same time period. Herein, we propose a method to quantify the myocyte content throughout the ECM patch region. We then investigate the relationship between the myocyte content within the patch region and the mechanical function generated by the region. We hypothesized that the repair of a right ventricular defect with acellular ECM increases myocyte content over time and that this increase correlates with the mechanical function generated within the region.

[1]Institute for Molecular Cardiology; [2]Diabetes and Metabolic Diseases Research Program; Departments of [3]Biomedical Engineering, [4]Surgery, and [5]Physiology and Biophysics; Stony Brook University, Stony Brook, New York.
[6]Department of Biomedical Engineering, Columbia University, New York, New York.
[7]McGowan Institute for Regenerative Medicine, University of Pittsburgh, Pittsburgh, Pennsylvania.
[8]Department of Biomedical Engineering, Worcester Polytechnic Institute, Worcester, Massachusetts.

Materials and Methods

Experimental design

All animals used in this study received humane care in compliance with an approved protocol by the IACUC committee at Stony Brook University and with the "Principles of Laboratory Animal Care" formulated by the National Society for Medical Research and the "Guide for the Care and Use of Laboratory Animals" prepared by the National Academy of Sciences and published by the National Institutes of Health (Bethesda, MD; NIH Publication No. 85-23, revised 1985).

Seventeen adult mongrel dogs weighing 20–30 kg were divided into three groups representing different survival times after implantation of a myocardial patch. The patch was made from a single layer of lyophilized ECM derived from the porcine urinary bladder[4] (ACell Vet V1023-LY; ACell, Jessup, MD). The time points studied were 0, 2, and 8 weeks consisting of four, four, and nine dogs, respectively. In the 0-week group, the patch was surgically implanted, followed by a 15-min recovery period and subsequent evaluation of mechanical function. In the 2- and 8-week groups, the chest was closed following patch implantation, and the animals were allowed to recover for the designated time period. A fourth group representing the baseline global function of the right ventricle (RV) was created from the four dogs in the 0-week group and four additional dogs used in another study.[8] Baseline sonomicrometry measurements were recorded from these eight dogs prior to defect creation and patch implantation, representing normal global RV function.

Surgical methods

The animals were sedated, intubated, and placed under general anesthesia using inhalational isofluorane. A fluid-filled pressure transducer was inserted into the femoral artery to monitor systemic blood pressure. A right thoracotomy was performed to expose the right ventricle, and a pericardial cradle was constructed.

The defect creation and subsequent repair with the ECM scaffold were as follows. While maintaining hemodynamics, a vascular clamp was used to isolate a portion of the right ventricular-free wall. A full-thickness portion of myocardium, approximately 10×15 mm in size, was excised from the right ventricle. An approximately 17×20 mm piece of ECM (100–150 μm in thickness) was used to repair the defect with a running 5-0 prolene suture. The clamp was released. If needed, gentle pressure or 5-0 prolene stitches were used to acquire adequate hemostasis. For the dogs in the 2- and 8-week groups, the chest was closed in layers, and the systemic pressure catheter was removed.

Prior to defect creation in the dogs comprising the baseline group, three pairs of sonomicrometry crystals (Triton, San Diego, CA) were implanted. The crystals were stitched to the heart to measure the distance along the baso–apical, anterior–posterior, and right ventricular-free wall–septal axes. Following the sonomicrometry measurements, lidocaine was administered to prevent arrhythmias, the defect was created, and the ECM scaffold was implanted as described in the previous paragraph. Following an approximate 10-min recovery period, global and regional RV mechanical function was measured.

Following the 2- and 8-week recovery periods for the 2- and 8-week groups, the animals were returned to the operating room, medicated, intubated, and placed under general anesthesia. Systemic pressure was again monitored through an arterial line in the femoral artery. The heart was exposed via a bilateral thoracotomy. Adhesions were carefully dissected off the heart to expose the patch and its suture line. A pressure transducer (Millar Instruments, Houston, TX) was placed into the RV through the right atrium. For dogs receiving global function measurements, sonomicrometry crystals were implanted as described in the previous paragraph.

Measurement of global function

Systolic function in the right ventricle was assessed using a modified ellipsoidal shell subtraction model of right ventricular volume (RVV)[9] and the linearity of the Frank–Starling relationship. The volume of the RV can be computed from measurements along three axes by the implanted sonomicrometer crystals minus the right ventricular-free wall volume (FWV):

$$\mathrm{RVV} = \pi/6 \times \mathrm{BA} \times \mathrm{AP} \times \mathrm{RVS} - \mathrm{FWV} \tag{1}$$

The RVV modeled as an ellipsoidal shell is a function of the distance from base to apex (BA), anterior to posterior (AP), and right ventricle-free wall to septum (RVS) of the right ventricle. We assumed FWV to be a constant value for each heart[9] (which would therefore not contribute to the determination of stroke work) for the purpose of our calculations and used the following equation:

$$\mathrm{RVV_{mod}} = \pi/6 \times \mathrm{BA} \times \mathrm{AP} \times \mathrm{RVS} \tag{2}$$

Pressure–volume loops were generated from the distance measures obtained by sonomicrometry and RV pressure samples as determined by the pressure transducer inserted into the right ventricular cavity. The work for each cardiac cycle was computed as

$$\mathrm{SW} = \int P \times \mathrm{d}V \tag{3}$$

The stroke work (SW) performed by the right ventricle during a cardiac cycle was computed as the integral of RV pressure (P) with respect to the derivative of RV volume (V).

Discrete integration was performed in custom-written software to compute stroke work values for each cardiac cycle. To provide a range of RV end diastolic volumes, the vena cava were transiently occluded during data acquisition. Stroke work was plotted against end diastolic $\mathrm{RVV_{mod}}$ (commonly referred to as the preload recruitable stroke work relationship) for each RV cardiac cycle, and a linear fit was performed using Excel (Microsoft, Redmond, WA). The slope of the line, M_w, represents right ventricular contractility, a measure of systolic function independent of heart rate and afterload.[9]

Measurement of regional mechanical function

Regional function was determined by high-density mapping (HDM) as described in detail elsewhere.[10,12] Briefly, silicon carbide particles (approximately 40 μm in diameter) were applied to the epicardial surface of the heart to create a

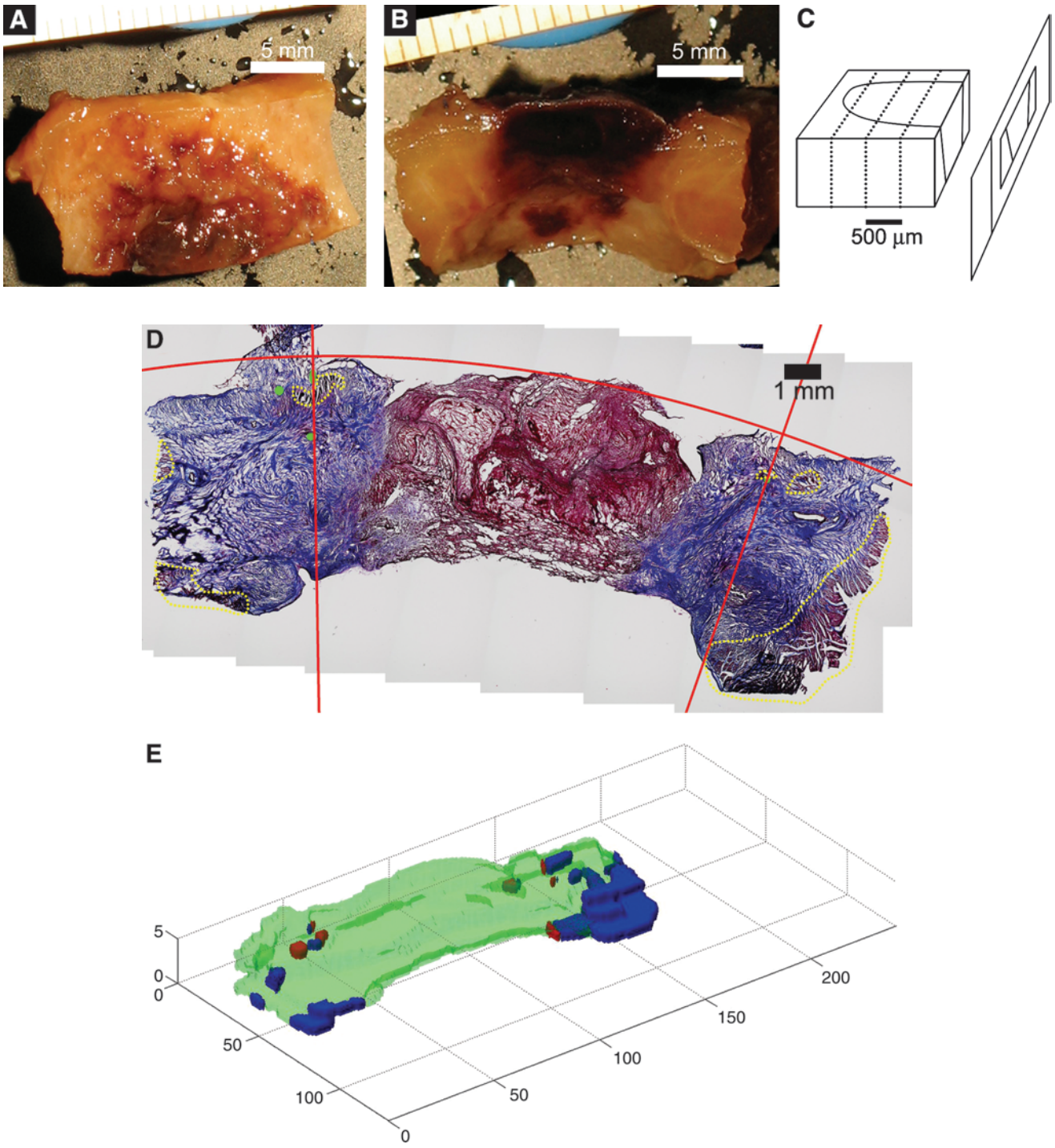

FIG. 1. (**A**) Epicardial and (**B**) transmural surface of one half of a 2-week ECM patch. (**C**) Diagram indicating how the patch region is sectioned along the plane parallel with the transmural surface. (**D**) Mosaic image of 2-week patch cross section stained with Masson's trichrome with myocyte regions outlined with dotted yellow lines. Green circles indicate suture locations, and red lines indicate the computed patch boundaries such that the region within the red lines is the patch region. The normal myocardium is only seen on the far ends of the image. The fibrotic region (blue) appears to localize with the area where the cross clamp was placed at the time of patch implantation. The red region in the center of the image appears to consist mostly of blood clots, with few myocytes in this region. The myocytes were mostly found surrounded by fibrotic tissue in the implantation zone. (**E**) Three-dimensional reconstruction of the patch region where neighboring myocardium is indicated by blue, myocyte regions within patch boundary are red, and nonmyocyte scar regions are translucent green.

random light intensity pattern. A complementary metal-oxide semiconductor camera (Photron, San Diego, CA) was focused on the region of interest (ROI) that contained the patch as defined by the 5-0 prolene sutures. Images were acquired at 125 frames/s over 7 s, and synchronous RV pressure readings were digitally recorded from the Millar pressure transducer via an analog-to-digital converter (National Instruments, Austin, TX).

Using a subpixel-extended phase correlation algorithm, displacements of the epicardial surface during the cardiac cycle at multiple locations within the ROI were obtained. Based on these displacements, the change in regional area within the ROI was determined. RSW was calculated by integrating RV pressure with respect to the area change. RSW was normalized to developed pressure and end diastolic regional area, yielding a unitless value. RSW is an index of the amount of work being performed by the region. As the closed line integral is path dependent, a positive value of RSW suggests that the region is contracting in synchrony with normal myocardium and thereby performing work. A negative value suggests that the environment is performing work on the region (i.e., deforming it out of synchrony with the normal contracting myocardium). SC, a measure of the area change during systole, was computed as the difference between end diastolic area and end systolic area of the ROI, normalized to end diastolic area.

Histology

Tissue samples consisting of one half the patch region and approximately 1 cm of surrounding myocardium (Fig. 1A, B) were obtained following the measurement of function, fixed in 4% paraformaldehyde overnight, switched to 30% sucrose for at least 12 h, and embedded in Jung tissue-freezing medium (Leica Microsystems Nussloch, Wetzlar, Germany) and frozen to -20°C. The prolene sutures were left intact for identification of the patch region boundaries. The samples were serially sectioned at 10 μm thickness in a cryostat and plated on numbered slides (Fig. 1C). Each section's serial number, the slide number that each section was plated onto, and every lost section were recorded to determine the tissue depth of each section.

Tissue sections were stained with either hematoxylin and eosin (H&E) or Masson's trichrome stain to identify histologic structure. Cardiomyocytes were identified immunohistochemically using a primary monoclonal sarcomeric α-actinin antibody (cat#: A7811; Sigma-Aldrich, St. Louis, MO). Sections were then incubated with a biotinylated anti-mouse secondary antibody (cat#: PK-7200; Vector Laboratories, Burlingame, CA). This incubation was followed by either (1) application of an avidin and biotinylated horseradish peroxidase complex, and then a DAB chromogen followed by hematoxylin counterstaining, or (2) application of streptavidin-conjugated quantum dots (cat#: 80-0004; Invitrogen, Eugene, OR) followed by nuclear labeling with Hoechst 33342 Dye (cat#: PA-3014; Cambrex, East Rutherford, NJ).

Recent studies have documented the possibility of myocyte proliferation contributing to cardiac regeneration. Therefore, to determine if myocyte proliferation might contribute to regeneration of myocytes in the implant region, sections were stained for cell cycle markers with a TRITC-conjugated antibody for Ki-67 (Santa Cruz Biotechnology, Santa Cruz, CA). In addition, as myocardium is known to exhibit a nontrivial amount of autoflorescence,[11] sections were also stained with HRP secondary antibodies to confirm Ki-67 and actinin staining.

Quantification of myocyte content

One half of the patch region from three 8-week and three 2-week ECM implants was processed for quantification of myocyte content. At least three tissue sections uniformly separated by approximately 500-μm intervals from each sample were stained with Masson's trichrome stain, and adjacent sections were stained for sarcomeric α-actinin and ventricular myosin heavy chain. Slides were imaged on an Olympus IX51 inverted microscope, (Olympus, Center Valley, PA) with an attached digital camera. Mosaics spanning the 1×3 cm tissue sections were created as follows: a series of approximately 40 overlapping images spanning the tissue sections were acquired at 680×512 pixel resolution using a 4× objective; subsequently the photomerge feature of Adobe Photoshop (version 8.0; Adobe Systems, San Jose, CA) was used to combine the images into a large mosaic image of the entire tissue section with a 4800 times; 2600 pixel resolution (Fig. 1D).

From each tissue section, mosaic image (1) regions containing myocytes and (2) tissue regions not containing myocytes were identified. The regions composed of myocytes were identified morphologically and traced using Adobe Photoshop (Fig. 2). The remaining tissue regions were identified as the tissue regions not containing myocytes. Adjacent serial tissue sections stained for sarcomeric α-actinin were used to confirm the presence of cardiomyocytes. Prior to staining, each slide was imaged and a mosaic was created containing cross sections of the sutures used to stitch the patch periphery to the neighboring myocardium. Because the staining process washed away the sutures, the prestaining mosaics were used to identify the Cartesian coordinates of the suture locations in the stained sections, allowing for identification of patch borders.

Following identification of the regions containing myocytes and suture coordinates, custom software written in Matlab (version 7.3; MathWorks, Natick, MA) was used to fit a second-order curve to the epicardial surface of each tissue section, defining the top boundary of the patch region. The left and right boundaries of the patch region were defined by two lines computationally determined to contain the left and right suture coordinates, respectively, and intersect the top boundary at the point, where a perpendicular angle was formed with the computed line and the tangent to the epicardial curve (Fig. 1D).

To quantify the cellular regions in the mosaics, the Red Green Blue (RGB) color image was converted to grayscale. Void regions, representing extracellular space, presented in white, as opposed to cellular regions that stained red or blue. The Matlab function gray thresh was used on each image to compute the threshold pixel value used to create a binary version of the image where pixels were classified as either representing a region of tissue or a region not containing tissue. The pixels representing tissue within the computed boundaries were tallied for each histologic section.

The average area occupied by myocytes per histologic section within the patch boundaries was used as the measure of myocyte content within each patch sample. Reddish and

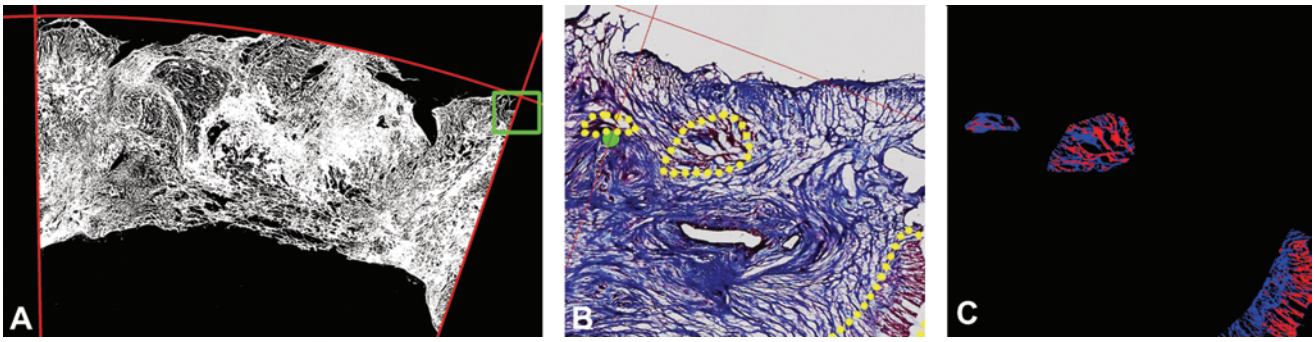

FIG. 2. (**A**) Tissue within the patch region boundaries (red lines) is indicated in white. The green box circumscribes the region shown at higher magnification in panels (**B**) and (**C**). (**B**) Dotted yellow lines outline myocyte-containing regions, and red lines indicate top and right patch region boundaries. (**C**) Reddish and bluish pixels within the respective hue ranges in each myocyte region are shown as either red or blue, accordingly.

bluish pixels were determined by first converting the RGB image to the hue saturation value color space. Hue values of reddish and bluish tissue regions were observed in multiple images of trichrome-stained slides, and mutually exclusive ranges of values containing all the reddish and all the bluish pixels were selected. The reddish pixels within identified myocyte regions were identified as comprising myocytes, and bluish pixels represented scar tissue. The pixel to metric scaling factor was determined and used to calculate the area in μm^2 comprised by the tallied reddish pixels. The number of reddish pixels within each traced myocyte region (Fig. 2) within the patch boundaries was tallied for each histologic section, and the average myocyte area was computed from at least three uniformly spaced histologic sections per patch sample.

To quantify the diameter of myocytes within the implant zone, longitudinal myocytes with discernable lateral borders were identified from microscopic images of H&E- and trichrome-stained histological sections. The distance spanning the lateral borders and perpendicular to the longitudinal axis of each identified myocyte was measured with ImageJ (version 1.37v; National Institutes of Health) and recorded as the myocyte diameter.

Three-dimensional reconstructions

The patch region and nearby neighboring myocardium was three-dimensionally reconstructed using Matlab from a minimum of three sections per tissue sample (Fig. 1). Myocyte and nonmyocyte regions were identified as described in the previous section, and binary masks were created identifying the regions. Three different image stacks per tissue sample were created from the binary images in Matlab representing the neighboring myocardium, myocyte regions within the patch boundaries, and regions of nonmyocyte scar area. Isosurfaces encompassing the volume of each stack were created and visualized with the Matlab patch command.

Statistical analysis

Statistical analysis was performed using Microsoft Excel with the Analysis Toolpack add-in (version 2003; Microsoft) and the Matlab Statistics toolbox (MathWorks). All data are presented as mean $\pm$ standard error of the mean. One-way analysis of variance (ANOVA) was used to determine whether there was a difference in right ventricular contractility as measured by M_w, between the baseline, 0-week, and 8-week groups. ANOVA was also used to determine if the values for RSW and SC were different between any of the 0-, 2-, and 8-week groups. A *post hoc* Tukey test was then used to perform multiple pair-wise comparisons. A two-sample *t*-test assuming equal variances was used to determine differences between the myocyte area/section ratios of the 2- and 8-week groups. Differences were considered significant for $p \leq 0.05$. Linear regression was used to determine how the dependent variables RSW and SC were affected by the independent variable myocyte area/section.

Results

Gross morphology

Following implantation, the ECM scaffold and the prolene sutures identifying the outer boundary of the patch were visible. Examination of cross sections of the ECM patch regions sacrificed approximately 2 h after implantation showed that the ECM scaffold was at the midmyocardial level, equidistant between the native endocardial and epicardial surfaces (Fig. 3).

Two weeks later, adhesions were present on the epicardial surface of the patch. Once removed, the patch region and surrounding sutures were apparent, but the ECM material was no longer discernable (Fig. 3). Cross sections of the 2-week patch revealed substantial thickening of the patch region due to the deposition of host tissue comprised of collagen, fibrin, and multiple cell types. At 8 weeks, the epicardial surface of the patch again contained adhesions that once removed revealed a patch region well integrated into the neighboring myocardium. Measurements made from the histological cross sections revealed that the ECM bioscaffold patch region was thinner, although not statistically significant ($p = 0.08$) at 8 weeks, decreasing from $5800 \pm 497\,\mu m$ at 2 weeks to $3357 \pm 935\,\mu m$ at 8 weeks.

In both the 2- and 8-week implants, a region of fibrosed tissue was seen around the edge of the implants. Among the reasons for the fibrosed tissue could be ischemia caused either by the cross clamping of this region during patch implantation or the placement of sutures in this region. Thus, suture location was used to calculate the implant border, rather than the change is tissue structure.

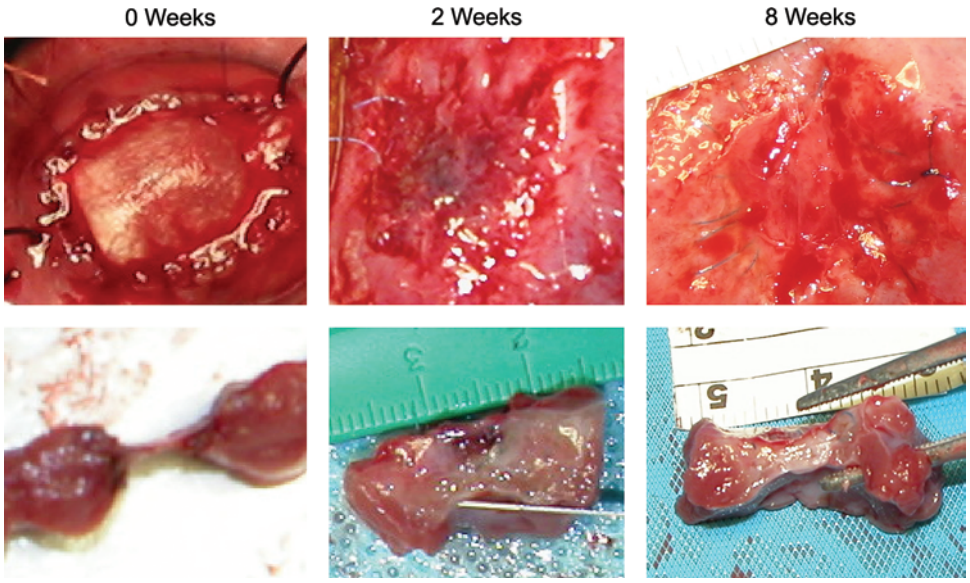

FIG. 3. Epicardial (top panels) and transmural (bottom panels) views of the ECM patch region 0, 2, and 8 weeks following implantation. Color images available online at www.liebertonline.com/ten.

Global mechanical function over time

Contractility of the entire right ventricle as measured by M_w was 1.9 ± 0.2 J/L at baseline ($n = 8$), 1.3 ± 0.2 J/L in the 0-week ($n = 4$), and 1.7 ± 0.2 J/L in the 8-week ($n = 4$) groups. There were no significant differences between these groups, likely due to the small size of the defect created (approximately 1.5×1.0 cm^2), which represents approximately 5% of the entire right ventricle.

Regeneration of regional mechanical function over time

The mean RSW of the ECM implant was $-0.5 \pm 1.4\%$ immediately after implantation ($n = 4$), with $-4.2 \pm 1.6\%$ SC (Fig. 4).

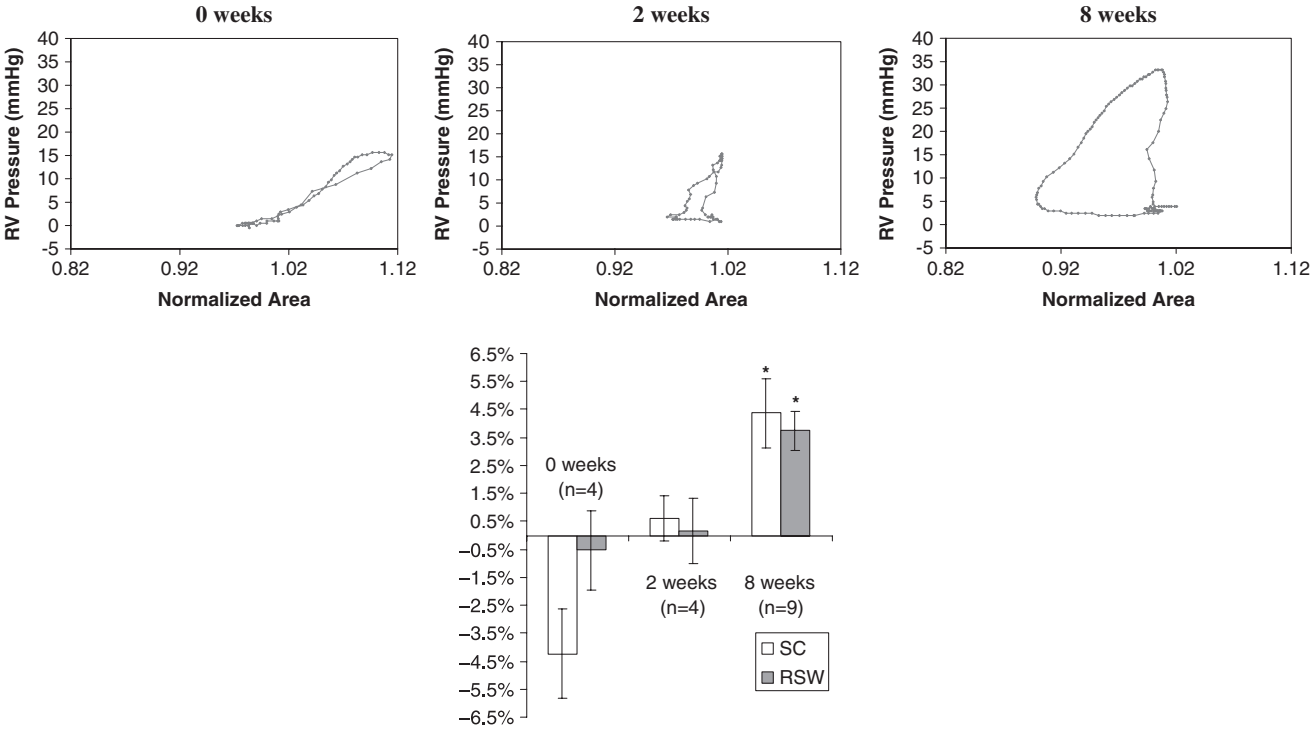

FIG. 4. Top panels show plots of right ventricular pressure versus area for the patch regions of a representative 0-, 2-, and 8-week ECM patch. Area at end diastole is normalized to one. The loops at 8 weeks progressed in a counterclockwise direction and indicated greater RSW relative to 2 and 0 weeks as can be seen by the larger area within the 8-week loop. The bottom panel shows a chart of mean SC and RSW values for the all the dogs in the 0-, 2-, and 8-week groups (*$p \leq 0.05$ vs. 0 week).

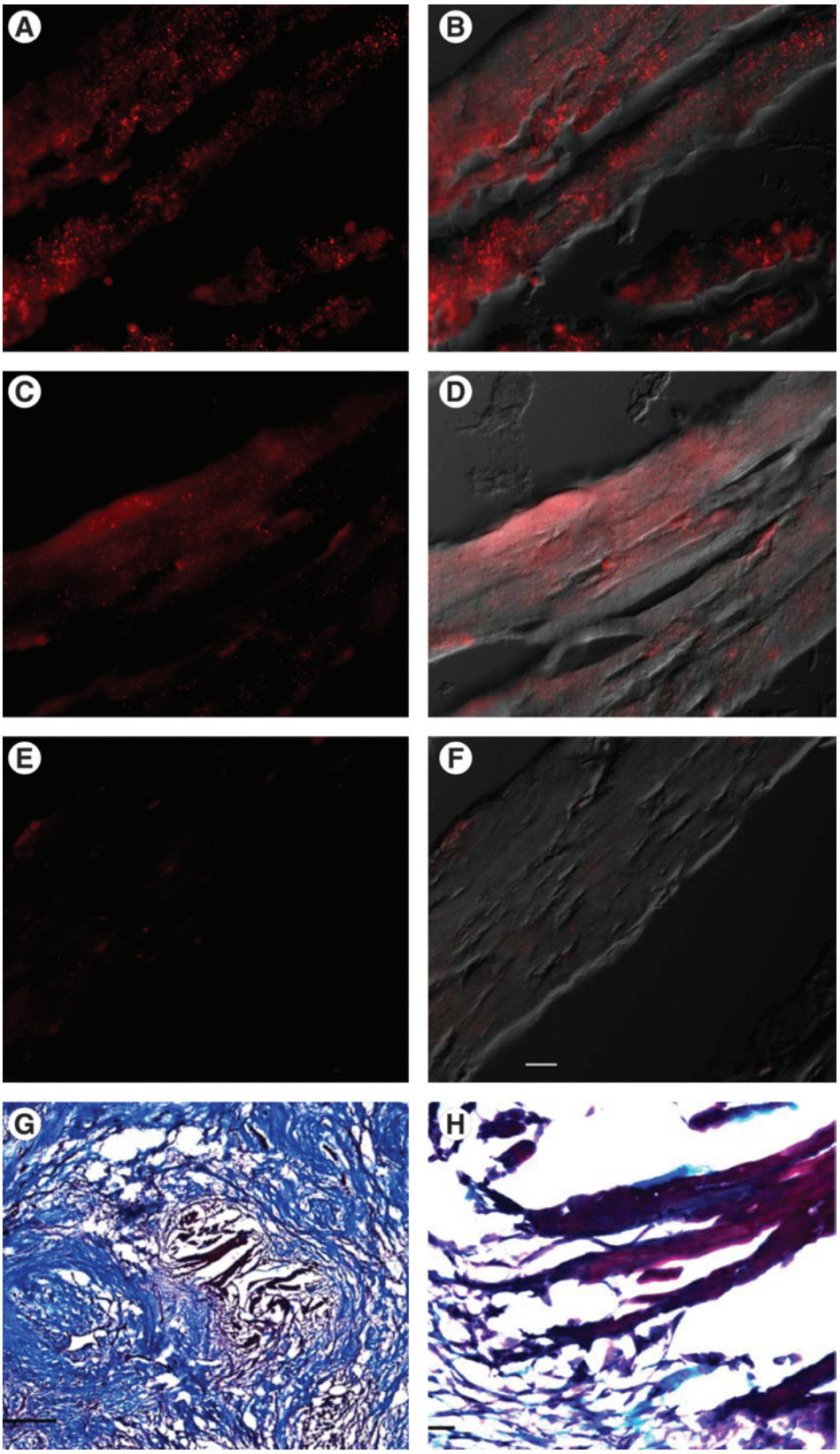

FIG. 5. Actinin, myosin heavy chain, trichrome, and control (no primary antibody) staining of myocytes from serial sections within the scaffold region 2 weeks after implantation of UBM. (**A**) Sarcomeric α-actinin staining (red; Qdot 655 secondary) of an island of myocytes within the urinary bladder matrix (UBM) implantation region. (**B**) Sarcomeric α-actinin staining combined with differential interference contrast (DIC) image. (**C**) Ventricular myosin heavy chain staining (red; Qdot 655 secondary) from a serial section to that shown in panel (**A**). (**D**) Ventricular myosin heavy chain staining combined with DIC image. (**E**) Control (no primary antibody) staining from a serial section to that shown in panel (**A**). (**F**) Control staining combined with DIC image. (**G**) Low-magnification image of trichrome-stained region within the implant boundary. Scale bar equals 0.5 mm. (**H**) Higher magnification of image in panel (**G**). Scale bar equals 50 μm for panels (**A–F**) and (**H**).

This result demonstrates that upon implantation, there is no regional work being done by the ECM implant, and the increase in load on the patch during systole (resulting from an increased RV pressure and stress exerted by contracting neighboring myocardium) results in passive deformation of the ECM patch (Fig. 4). This result was expected due to the relatively high compliance of the ECM material as compared to the neighboring myocardium.

Two weeks after implantation, the remodeled ECM patch had near-zero SC ($0.6 \pm 0.8\%$; $n = 4$) and RSW ($0.1 \pm 1.2\%$; $n = 4$). The regional area workloop of the 2-week ECM patch demonstrated less change in area than the 0-week patch (Fig. 4), which indicates that the patch region is deformed less by the stresses generated from the RV pressure and contracting neighboring myocardium. This result suggests that the compliance of the patch region decreased between 0 and 2 weeks, likely due to the tissue buildup and increased thickness of the region.

Eight weeks postimplantation, both the SC and RSW values had increased significantly to $4.4 \pm 1.2\%$ ($n = 9$) and $3.7 \pm 0.7\%$ ($n = 9$), respectively. The SC values measured in the 8-week ECM are approximately one-fifth of $21.6 \pm 1.2\%$, the mean value recorded for normal healthy RV in a previous study.[6]

The difference between the RSW values at 2 and 8 weeks approached significance ($p = 0.051$), while the difference between 2- and 8-week SC values was not significant ($p = 0.17$). The 8-week patch region demonstrated an iso-volumic systolic phase followed by a decrease in regional area that continued into diastole (Fig. 4). The decrease in regional area during systole indicates active contraction of the patch region in synchrony with the neighboring myocardium, which suggests the presence of contractile myocardium within the region.

Histology

Myocytes were identified within the patch boundaries in serial sections based on their morphology. In serial sections, cells within these same regions stained positive for sarcomeric actinin and ventricular myosin heavy chain (Fig. 5).

In both the 2- and 8-week patches, trichrome-stained cross sections spanning from the neighboring myocardium on one side of the patch to the neighboring myocardium on the opposing side revealed collagen interspersed with islands of myocytes (regions of myocytes separated from the neighboring myocardium by collagen) both inside and outside the computed patch boundaries. The morphology and organization of the myocytes in the 8-week islands appeared similar to the neighboring myocardium (Fig. 6). The myocytes in many of the 2-week islands appeared morphologically distinct from the myocytes in the 2-week neighboring myocardium, which was similar to the 8-week neighboring myocardium. The myocytes in the 2-week islands appeared more amorphous, often lacked distinct striations, and nuclei were less visible than in the neighboring myocardium (Fig. 6).

In most cross sections, the contiguous neighboring myocardium was outside the computed patch boundary. However, in one 2-week and one 8-week patch, the neighboring myocardium tapered through the computed boundary into the patch region, possibly due to the myocardium being cut at an acute or obtuse angle (not orthogonal) during defect creation. Within these regions of neighboring myocardium, two morphologically distinct regions were observed. In the re-

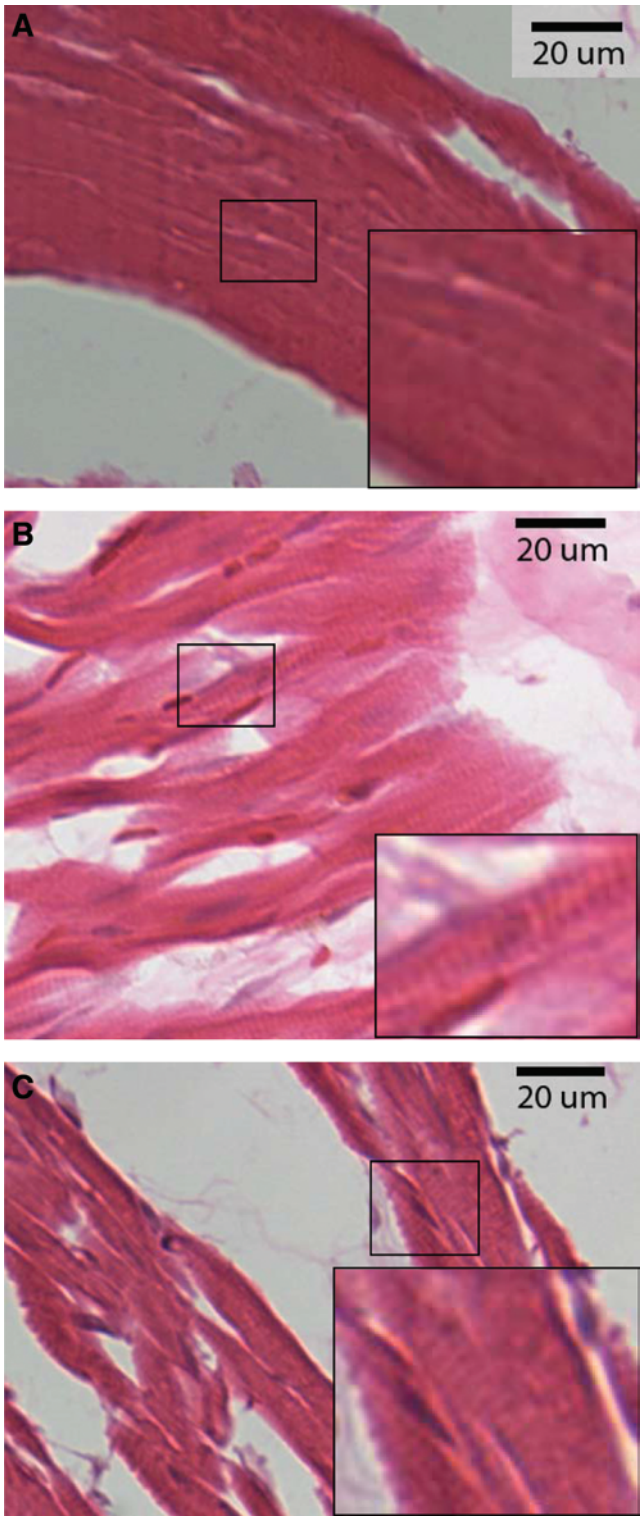

FIG. 6. H&E-stained myocytes from a 2-week island (**A**), an 8-week island (**B**), and native myocardium neighboring the 2-week patch region (**C**) from the same histological section as the island shown in (**A**). Sarcomeres were not visible in the myocytes in the 2-week islands (**A**, inset) but were visible in the myocytes in 8-week islands (**B**, inset), and native myocardium neighboring the 2-week patch (**C**, inset). Color images available online at www.liebertonline.com/ten.

gions extending from the neighboring myocardium into the patch region, the myocytes appeared normal and had fiber orientations consistent with the rest of the neighboring myocardium. At the tip of these tapering regions, the myocytes appeared smaller and morphologically dissimilar to the other myocytes in the neighboring myocardium. Their orientations also became more varied and discontinuous from the neighboring myocardium outside of the suture boundaries. For the quantification of myocyte content, the region of neighboring myocardium containing the myocytes that were continuous and morphologically similar to the neighboring myocardium was excluded from the quantification of myocyte content within the patch.

The three-dimensional reconstructions of the 2- and 8-week patches demonstrated regions of neighboring myocardium (Fig. 7) predominantly outside the patch boundaries. Islands of myocytes were located partly inside (Fig. 7, red) and outside (Fig. 7, blue) the computed boundaries.

Myocyte content increases from 2 to 8 weeks

Diameters of individual myocytes were measured as an indication of myocyte size. Diameters of 20 myocytes in myocyte islands were measured from histologic sections from each of the three 2-week and three 8-week dogs totaling measurement of 60 myocyte diameters for the 2-week group and 60 diameters for the 8-week group. The average myocyte diameter was calculated for each group by averaging the average myocyte diameter calculated from each dog in that group.

The average diameter of myocytes in the 8-week islands was $6.2 \pm 0.1\,\mu m$, significantly less than the myocyte diameter of $9.3 \pm 1.1\,\mu m$ in the 2-week islands ($p < 0.05$) (Fig. 8). An average diameter of $10.9 \pm 1.0\,\mu m$ was calculated from the myocyte diameter of normal RV from three different dogs, where each dog's myocyte diameter was an average from 20 myocytes from that dog, totaling 60 myocytes total from normal RV.

While the average diameter of myocytes was smaller in the 8-week islands, the average area per histologic section within the patch boundaries occupied by myocytes increased significantly from $221{,}149 \pm 50{,}352\,\mu m^2$ at 2 weeks to $470{,}666 \pm 49{,}192\,\mu m^2$ at 8 weeks (Fig. 8). The two-dimensional area occupied by individual myocytes was not calculated due to the difficulty in determining complete boundaries of myocytes. However, the end-to-end length of myocytes in the 8-week islands did not appear greater than that in the 2-week islands. Although measurements of myocyte diameter have serious methodological limitations, the differences in these measurements suggest, at the very least, that the increases in myocyte area observed at 8 weeks compared to 2 weeks represent some degree of myocyte hyperplasia rather than hypertrophy.

Mechanical function is correlated with the myocyte content within the patch region

Linear regression analysis was used to investigate the correlation between regional patch function and the myocyte content within the patch. Linear regression of RSW and SC generated by each patch region with respect to the average

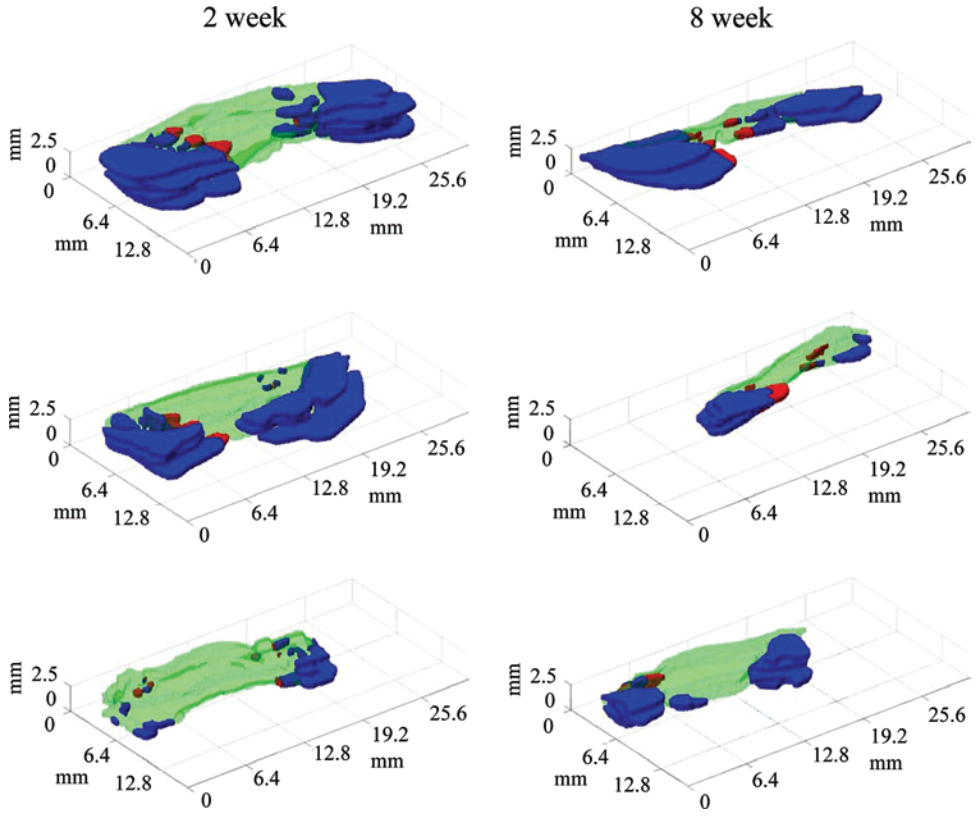

FIG. 7. Three-dimensional reconstructions of three 2-week (left column) and three 8-week (right column) patch regions. Blue indicates regions of myocytes outside of the computed patch boundaries, red indicates myocyte regions within the patch boundaries, and green indicates nonmyocyte scar throughout patch. Color images available online at www.liebertonline.com/ten.

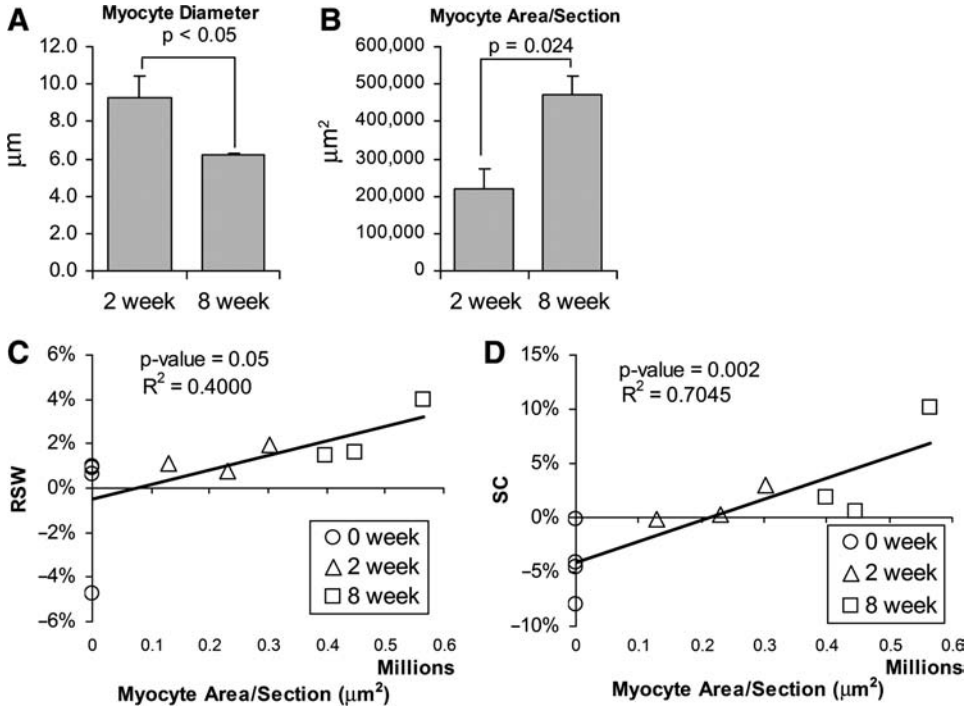

FIG. 8. (**A**) The average diameter of myocytes within the patch regions decreased from 2 to 8 weeks. (**B**) The average area per histologic section within the patch boundaries occupied by myocytes increased from 2 to 8 weeks. (**C**, **D**) The relationship between RSW versus myocyte area/section and SC versus myocyte area/section fit the linear relationship indicated in the plots where goodness of the fit is indicated by the R^2-values. The p-values from the regressions are ≤ 0.05, indicating a significant correlation between the variables and myocyte area/section.

myocyte area per section for each patch demonstrated a positive linear relationship for both parameters. Both linear relationships were significant (RSW vs. area: $p = 0.05$; SC vs. area: $p = 0.002$). SC versus myocyte area per section more closely fit a linear relationship than RSW versus myocyte area, as indicated by the greater R^2-value and the smaller p-value (Fig. 8).

Evidence of myocyte proliferation within the urinary bladder matrix (UBM) implant region

To determine if myocyte proliferation was in part responsible for the regeneration in the UBM implant region, we examined 8-week UBM implants for expression of a marker of cell division, Ki-67. This marker was absent in neighboring myocardium adjacent to the implant area, demonstrating that this region was composed of mitotically silent myocytes. However, we found numerous small cells surrounding islands of myocytes with in the patch border at 2 weeks that were Ki-67 positive (Fig. 9). Many of the small cells also stained positive for the cardiac marker sarcomeric α-actinin. Similar results were seen using an HRP secondary antibody, reducing the possibility of autofluorescence contributing to the findings. Cell cycle marker staining was much less prevalent in the 8-week implants than in the 2-week implants. Many of the cells staining positive for cell cycle markers did not appear to be myocytes, and most of the small cells staining positive for cell cycle markers and actinin were not striated.

Discussion

A method was developed to measure myocyte content within a full-thickness region of myocardium replaced by an ECM-based scaffold. Measurements made with this method demonstrate that myocyte content increased from 0 to 2 and then again to 8 weeks within the region. The effect myocyte content within a patch region had on the mechanical function was investigated, demonstrating that increased function was linearly correlated with increased myocyte content. This study expands on previous studies demonstrating ECM-induced regeneration of mechanical function[4,6] by demonstrating that the measured function is associated with myocyte content, an aspect of the region's structure. The increased area of myocytes per section within the patch region combined with the smaller diameters of the myocytes at 8 weeks is suggestive of ECM-induced expansion of myocyte number and functionally significant myocardial regeneration.

One of the issues associated with myocardial regeneration is the resultant production of mechanical function. The defect created in the right ventricle, approximately 5% of the right ventricle, is probably too small to result in significant changes in global ventricular function.[6] By using the high spatial resolution and accuracy associated with HDM,[12] we are able to study mechanical function within the patch region while minimizing many of the deleterious effects associated with global cardiac dysfunction. Future studies will focus on the more clinically relevant issue of myocardial infarction to determine if regeneration can occur with the compounding deleterious effects of infarction, including global dysfunction.

While myocytes may be regenerated, they must still be able to deform their substrate to provide useful mechanical work. HDM is able to determine regional deformation within the patch boundaries simultaneously with ventricular pressure. From these data, it can be determined if the region is actively contracting in sync with the rest of the myocardium. When the material is implanted and there are no contractile cells present (0 week; Fig. 4), the passive material increases in area with an increased intracavitary load. However, 2 weeks after implantation, cells are present. As can be seen in Figure 8, zero RSW or SC is associated with a small level of myocyte content within the patch. This linear fit suggests that less than approximately 225,000 μm^2 of myocyte area (per section) within the patch region is insufficient for generation of measurable positive SC. The patch region contains large amounts of

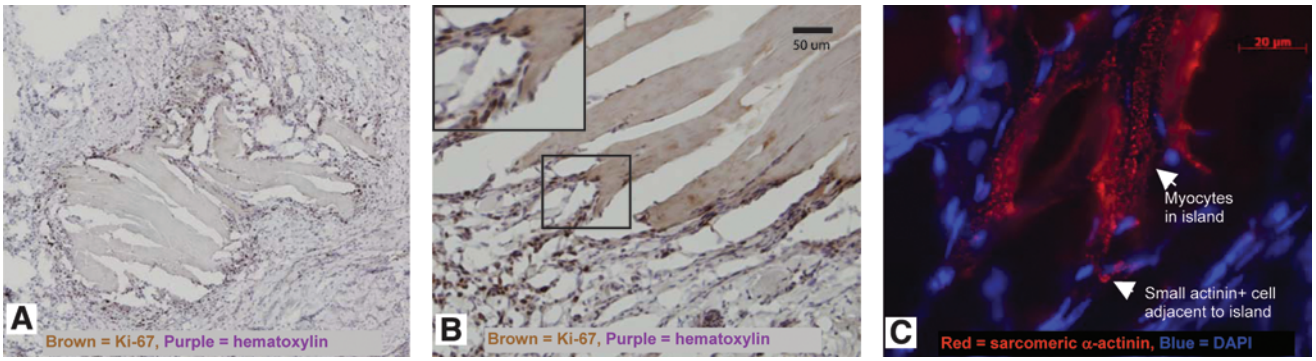

FIG. 9. Cell cycle markers are present in myocytes within the implant zone. (**A**) Island of myocytes surrounded by dense ring of small Ki-67+ cells shown with brown nuclei. (**B**) Border of island of myocytes showing higher magnification view of Ki-67+ cells appearing directly adjacent to longitudinal myocytes; inset in the upper left corner is a zoom in view of the area within the black box. (**C**) Some of the small cells in the ring stain positive for sarcomeric α-actinin shown in red.

collagen and other cell types that may provide too much resistance for a small number of contracting myocytes to overcome, preventing measurable contraction of the region, until a critical mass of myocytes is achieved. Further, myocytes must be electrically coupled to the rest of the myocardium to contract in the rhythmic synchronous pattern necessary to perform stroke work. Too few cells in a given volume may not provide sufficient coupling, preventing proper contractile function of the region.

Previous studies investigating myocardial regeneration using delivery of various cell sources into infarcts have demonstrated improvements in cardiac function and have documented the creation of new myocardium.[13,14] However, there is a need to measure total myocyte mass and individual myocyte size to determine whether myocyte regeneration is contributing to the improved function, as altering the passive mechanical properties of the myocardium may also lead to improved mechanical function.[15,16] The method developed in this study provides a means to measure myocyte content throughout the region utilizing uniform random sampling of the cross sections from which to make the measurements. A limitation of this study is that this method does not directly measure myocyte numbers. However, the decreased diameter of 8-week myocytes combined with the increased area per section occupied by myocytes strongly suggests an expansion of myocyte number within the patch region from 2 to 8 weeks, as opposed to myocyte hypertrophy. Also, the computed borders of the patch region, while calculated based on suture coordinates, are estimates of the actual borders and therefore may include some neighboring myocardium within the patch region.

The myocyte quantification results give rise to the following two questions. Where do the myocytes at 2 weeks originate? How does the myocyte content increase from 2 to 8 weeks? One possible source of the expansion of myocytes from 2 to 8 weeks could be the result of myocyte proliferation.

Following myocardial infarction, the heart does not reconstitute lost cardiomyocytes and the damaged tissue is eventually replaced by scar. However, this does not rule out the possibility of regeneration of mammalian heart in an environment different from that of the infarcted heart. For instance, noninfarcted zebrafish and amphibians regenerate amputated parts of the heart, and in amphibians, this occurs as a result of mitotic expansion of cardiomyocytes.[17,18] Ott *et al*. recently demonstrated that the rat heart could be regenerated by reseeding the ECM from the heart with cardiac myocytes, although they did not elucidate the mechanism involved in regenerating the heart.[19] Recent data, primarily from Anversa's lab, have suggested that myocytes can divide, and at rates that may be clinically relevant.[14,20] His laboratory has shown that myocytes reenter the cell cycle in regions bordering a myocardial infarction. This was indicated by their observation that 4% of myocytes in the border zone between the infracted and viable tissue stained positive for Ki-67, a nuclear protein involved in cell proliferation.[20] Other groups have also demonstrated relatively high myocyte proliferation rates.[21,22] Bone marrow–derived cells, subpopulations of which have demonstrated the ability to differentiate into myocytes, are attracted to the UBM scaffold[23] and may play a role in inducing myocyte proliferation. The increase in myocyte content measured in this study may be due at least in part to proliferation of myocytes adjacent to and within the patch region. However, we cannot rule out progenitor cell differentiation and/or myocyte migration as the cause of the increasing myocyte content in the patch region that occurs between 2 and 8 weeks postpatch implantation. Due to the lack of a unique specific marker to stain for myocardial progenitor cells, we only sought to identify cardiac myocytes.

The complex interplay of processes by which stem cells generate functional myocardium is not understood. Stem cells, however, are attracted to the site of injury[24] where they are exposed to the chemical, mechanical, and electrical signals present in the microenvironment. The microenvironment provided by the composition and three-dimensional ultrastructure of the ECM alone can affect cell function. Matsubara *et al*. demonstrated that human mesenchymal stem cells have an increased proliferation rate when grown on ECM as compared to that of plastic.[25] Polte *et al.* have demonstrated that ECM can affect cell adhesion.[25,26] Thus, it may be possible for the ECM patch to attract cardiac progenitor cells that will attach, proliferate, and possibly differentiate into functional myocytes.

It may also be possible for myocytes to migrate into the implant region from neighboring tissue. Determination of the boundary between the native myocardium and the biodegradable ECM scaffold is difficult; however, computing a

boundary based on a nonbiodegradable marker, the prolene sutures, and the tissue geometry allows computation of an objective boundary. This boundary, while an improvement over one subjectively determined, may be altered during the 8-week recovery period, thereby incorporating a quantity of neighboring myocardium inside the boundary line.

Future directions

Loss of healthy contractile myocytes due to pathological conditions can lead to heart failure. A treatment that could replenish the contractile elements in the heart would provide invaluable prevention of many heart failure–related deaths. ECM shows promise as a scaffold supportive of myocardial regeneration. The addition of exogenous cells that could differentiate into cardiomyocytes or release factors that stimulate myocyte proliferation could further enhance regeneration. The addition of cells may also limit postischemic remodeling.[27] Regardless of the methods used to induce regeneration, quantitative measures of the structure of the region in addition to the resulting function are needed to better evaluate the outcomes. The rules governing mammalian myocardial regeneration are not fully understood; however, further studies involving perturbations of the myocardial environment and quantitative measures of consequent structure and function will provide the insights necessary to engineer an environment favoring myocardial regeneration with the goal of reducing cardiac-related mortality.

Acknowledgments

This work was supported by the National Institutes of Health, HL67101 (I.S.C.), HL28958 (I.S.C.), an institutional grant from NYSTEM, EB000261 (S.F.B), Scientist Development Grants from the American Heart Association (G.R.G. and S.V.D), and an NIH training grant DK07521 (D.J.K).

Disclosure Statement

No competing financial interests exist.

References

1. Athanasuleas, C.L., Stanley, A.W., Jr., Buckberg, G.D., Dor, V., DiDonato, M., and Blackstone, E.H. Surgical anterior ventricular endocardial restoration (SAVER) in the dilated remodeled ventricle after anterior myocardial infarction. RESTORE group. Reconstructive endoventricular surgery, returning Torsion original radius elliptical shape to the LV. J Am Coll Cardiol **37,** 1199, 2001.
2. Ozawa, T., Mickle, D.A., Weisel, R.D., Koyama, N., Wong, H., Ozawa, S., and Li, R.K. Histologic changes of nonbiodegradable and biodegradable biomaterials used to repair right ventricular heart defects in rats. J Thorac Cardiovasc Surg **124,** 1157, 2002.
3. Cohn, L.H., and Edmunds, L.H. Cardiac Surgery in the Adult. New York: McGraw-Hill, Medical Pub. Division, 2003.
4. Badylak, S., Obermiller, J., Geddes, L., and Matheny, R. Extracellular matrix for myocardial repair. Heart Surg Forum **6,** E20, 2003.
5. Ozawa, T., Mickle, D.A., Weisel, R.D., Koyama, N., Ozawa, S., and Li, R.K. Optimal biomaterial for creation of autologous cardiac grafts. Circulation **106,** I176, 2002.
6. Kochupura, P.V., Azeloglu, E.U., Kelly, D.J., Doronin, S.V., Badylak, S.F., Krukenkamp, I.B., Cohen, I.S., and Gaudette, G.R. Tissue-engineered myocardial patch derived from extracellular matrix provides regional mechanical function. Circulation **112,** I144, 2005.
7. Robinson, K.A., Li, J., Mathison, M., Redkar, A., Cui, J., Chronos, N.A., Matheny, R.G., and Badylak, S.F. Extracellular matrix scaffold for cardiac repair. Circulation **112,** I135, 2005.
8. Badylak, S.F., Kochupura, P.V., Cohen, I.S., Doronin, S.V., Saltman, A.E., Gilbert, T.W., Kelly, D.J., Ignotz, R.A., and Gaudette, G.R. The use of extracellular matrix as an inductive scaffold for the partial replacement of functional myocardium. Cell Transplant **15 Suppl 1,** S29, 2006.
9. Feneley, M.P., Elbeery, J.R., Gaynor, J.W., Gall, S.A., Jr., Davis, J.W., and Rankin, J.S. Ellipsoidal shell subtraction model of right ventricular volume. Comparison with regional free wall dimensions as indexes of right ventricular function. Circ Res **67,** 1427, 1990.
10. Gaudette, G.R., Azeloglu, E.U., Oleszak, L., Saltman, A.E., Krukenkamp, I.B., and Chiang, F.P. Determination of regional area stroke work with high spatial resolution in the heart. Cardiovasc Eng Int J **2,** 129, 2002.
11. Laflamme, M.A., and Murry, C.E. Regenerating the heart. Nat Biotechnol **23,** 845, 2005.
12. Kelly, D.J., Azeloglu, E.U., Kochupura, P.V., Sharma, G.S., and Gaudette, G.R. Accuracy and reproducibility of a subpixel extended phase correlation method to determine micron level displacements in the heart. Med Eng Phys **29,** 154, 2007.
13. Amado, L.C., Saliaris, A.P., Schuleri, K.H., St John, M., Xie, J.S., Cattaneo, S., Durand, D.J., Fitton, T., Kuang, J.Q., Stewart, G., Lehrke, S., Baumgartner, W.W., Martin, B.J., Heldman, A.W., and Hare, J.M. Cardiac repair with intramyocardial injection of allogeneic mesenchymal stem cells after myocardial infarction. Proc Natl Acad Sci USA **102,** 11474, 2005.
14. Orlic, D., Kajstura, J., Chimenti, S., Jakoniuk, I., Anderson, S.M., Li, B., Pickel, J., McKay, R., Nadal-Ginard, B., Bodine, D.M., Leri, A., and Anversa, P. Bone marrow cells regenerate infarcted myocardium. Nature **410,** 701, 2001.
15. Gaudette, G.R., and Cohen, I.S. Cardiac regeneration: materials can improve the passive properties of myocardium, but cell therapy must do more. Circulation **114,** 2575, 2006.
16. Wall, S.T., Walker, J.C., Healy, K.E., Ratcliffe, M.B., and Guccione, J.M. Theoretical impact of the injection of material into the myocardium: a finite element model simulation. Circulation **114,** 2627, 2006.
17. Flink, I.L. Cell cycle reentry of ventricular and atrial cardiomyocytes and cells within the epicardium following amputation of the ventricular apex in the axolotl, Amblystoma mexicanum: confocal microscopic immunofluorescent image analysis of bromodeoxyuridine-labeled nuclei. Anat Embryol (Berl) **205,** 235, 2002.
18. Poss, K.D., Wilson, L.G., and Keating, M.T. Heart regeneration in zebrafish. Science **298,** 2188, 2002.
19. Ott, H.C., Matthiesen, T.S., Goh, S.K., Black, L.D., Kren, S.M., Netoff, T.I., and Taylor, D.A. Perfusion-decellularized matrix: using nature's platform to engineer a bioartificial heart. Nat Med **14,** 213, 2008.
20. Beltrami, A.P., Urbanek, K., Kajstura, J., Yan, S.M., Finato, N., Bussani, R., Nadal-Ginard, B., Silvestri, F., Leri, A., Beltrami, C.A., and Anversa, P. Evidence that human cardiac myocytes

divide after myocardial infarction. N Engl J Med **344,** 1750, 2001.
21. Oberpriller, J.O., Ferrans, V.J., and Carroll, R.J. DNA synthesis in rat atrial myocytes as a response to left ventricular infarction. An autoradiographic study of enzymatically dissociated myocytes. J Mol Cell Cardiol **16,** 1119, 1984.
22. Rumëiìanëtìsev, P.P., and Carlson, B.M. Growth and Hyperplasia of Cardiac Muscle Cells. London, UK; New York, NY: Harwood Academic Publishers, 1991.
23. Badylak, S.F., Park, K., Peppas, N., McCabe, G., and Yoder, M. Marrow-derived cells populate scaffolds composed of xenogeneic extracellular matrix. Exp Hematol **29,** 1310, 2001.
24. Abbott, J.D., Huang, Y., Liu, D., Hickey, R., Krause, D.S., and Giordano, F.J. Stromal cell-derived factor-1alpha plays a critical role in stem cell recruitment to the heart after myocardial infarction but is not sufficient to induce homing in the absence of injury. Circulation **110,** 3300, 2004.
25. Matsubara, T., Tsutsumi, S., Pan, H., Hiraoka, H., Oda, R., Nishimura, M., Kawaguchi, H., Nakamura, K., and Kato, Y. A new technique to expand human mesenchymal stem cells using basement membrane extracellular matrix. Biochem Biophys Res Commun **313,** 503, 2004.
26. Polte, T.R., Eichler, G.S., Wang, N., and Ingber, D.E. Extracellular matrix controls myosin light chain phosphorylation and cell contractility through modulation of cell shape and cytoskeletal prestress. Am J Physiol Cell Physiol **286,** C518, 2004.
27. Cortes-Morichetti, M., Frati, G., Schussler, O., van Huyen, J.P., Lauret, E., Genovese, J.A., Carpentier, A.F., and Chachques, J.C. Association between a cell-seeded collagen matrix and cellular cardiomyoplasty for myocardial support and regeneration. Tissue Eng **13,** 2681, 2007.

Address correspondence to:
Glenn R. Gaudette, Ph.D.
Department of Biomedical Engineering
Worcester Polytechnic Institute
Worcester, MA 01609

E-mail: gaudette@wpi.edu

Received: July 25, 2008
Accepted: December 12, 2008
Online Publication Date: February 10, 2009